Original Article

Integrating Solar Energy with Battery Storage Systems for Optimal Efficiency using Landsman Converter

Monika Khatri[1], Murali Matcha[2], Siddheswar Kar[3], Neha Verma[4], Sharda Patwa[5]

[1,2,3,4,5]*Department of Electrical Engineering, Medi-Caps University, Madhya Pradesh, India.*

[1]*Corresponding Author : monikakhatri1995@yahoo.com*

Abstract - As solar Photovoltaic (PV) power generation develops more commonly, its inherent intermittency poses a challenge in designing and implementing it for smart grids. With many deployed photovoltaic devices, grid-tied solar power generation is a dispersed resource. Its results may change quickly and cause many issues for the distribution system operator. Therefore, battery energy storage is often employed to assist in the grid integration of solar electricity. The optimal designs for Photovoltaic (PV) systems with Battery Energy Storage Systems (BEES) is proposed in this study. A Landsman converter is an even power transfer from the solar PV source to the AC grid. The BESS is connected to a DC connection by a bidirectional DC converter to store excess energy. The use of LC filters minimizes the harmonics. The MATLAB software simulates the output of the proposed work. As a result, the suggested technique achieves less THD value of 1.24% compared to the conventional approaches.

Keywords - PV system, BEES, Landsman converter, LC filters, MATLAB.

1. Introduction

The annual emissions growth of the transport sector is the reason for around 23% of all energy-related CO_2 emissions worldwide. In order to decarbonize the transportation industry, electrification is anticipated to be crucial. Battery Electric Vehicles (BEVs) and plug-in hybrid electric vehicles are being adopted at significantly higher rates due to their superior reliability, lower operating costs, decreased greenhouse gas emissions, improved battery technology, and driving range [1, 2].

Recently, distributed generating systems based on solar PV is become more prevalent as a means of supplying the increasing demand for energy while using fewer fossil fuels and addressing concerns about climate change[3]. The discontinuous structure and partial shadowing features of the delivered electricity are two primary difficulties caused by the increasing integration of Solar Photovoltaic renewable energy sources into the conventional power grid [4, 5].

Further equipment resources and working approaches, like improbability modelling or probabilistic optimization approaches, are needed to prevent the adverse effects of PVs on Microgrids (MGs). By minimizing the short-term swings in PV production, the BESS, a flexible, controlled device, is designed to address these issues. [6, 7]. Energy Storage Systems (ESSs) allow additional energy to be saved and returned when output exceeds use. In order to increase

residential prosumers' self-consumption, the addition of Photovoltaic with BESS is growing in popularity. Due to the resources' unending nature, complementarity, economic viability, environmental friendliness, and bi-directionality, the PV-BESS is a practical renewable choice [8, 9].

Fortunately, the advancement of energy storage expertise offers a novel approach to successfully resolving the temporal gap between the electricity depletion of residents and the generation of power by residential PVs as well as boosting the deployment of residential PVs [9] an effective charging system performance is provided by the power electronic converter. In order to produce virtually sinusoidal current absorption and controlled dc output voltage, the converter is required [11].

The traditional boost converter is the most basic dc-dc topology for increasing voltage. However, the high-duty cycle is necessary to increase the voltage. Therefore it does not give the optimal solution. Using a buck converter, the output voltage will be lower than the input voltage, and it can step down the voltage but not attain high gain due to its inefficiency in components [12, 13]. As a result, both Boost and Buck converters are unsuitable for constantly charging the battery in the case of PV system battery charging [14]. The buck-boost converter gives a lower operational duty cycle and enhanced efficacy among input and output voltages. It can step-up or step-down voltages with small

components. Cuk DC/DC converter can produce output voltages either greater or lesser than the input voltage from the Photovoltaic module. The SEPIC converter has a more excellent duty cycle and a more significant voltage transfer gain, and it is helpful in solar panel systems because it can maintain a constant output voltage even when the input voltage or load fluctuates. This is possible since the input voltage can shift significantly due to solar insolation or temperature variations.

Low output ripples are one feature of a Zeta converter that makes it easier to regulate output [15-18], .but; the abovementioned converters have poor efficiency, which leads to stress on the components. To overcome such problems, the proposed method utilizes the Landsman converter. The converters are controlled using PID controllers in conventional techniques, which are practical and convenient in many control sectors. However, it performs poorly when managing an integrating process and a lengthy time delay process. The steady-state error is decreased by using the PI and Fuzzy controllers [19-22]. However, it takes more time to settle and relies entirely on human expertise and understanding, which is the drawback of these controllers [23]. Therefore, the suggested method uses the cascaded Fuzzy controller.

In this study, the DC-DC landsman converter is utilized to enhance power quality from the PV system. A cascaded Fuzzy controller is employed to control the converter

voltage. The bidirectional converter is employed to charge and discharge the power. A bidirectional DC converter connects the BESS to the DC connector to balance the energy. The MATLAB software simulates the result. As a result, the proposed technique attains a Low THD value by using the Landsman converter compared to the other conventional converters.

2. Proposed Methodology

In solar Photovoltaics, irradiance is converted directly into electricity through solar cells, but it is affected by climatic conditions. Therefore the Landsman converter is utilized in this work to increase the DC voltage from the Photovoltaic system. A cascaded Fuzzy controller is employed to stabilize the voltage and improve the dynamic performance of Cascaded converters by providing error compensation, which enhances the output and the essential DC supply sent through the PWM generator into the converter. BESS is connected to a DC connection by a bidirectional DC converter to store excess energy.

P_{act}, Q_{act} and P_{ref}, P_{ref} are compared, and the error is given to the PI controller, which reduces the steady state error for the system stability and enhances the grid performance. The PI controller is fed to the PWM generator that generates pulses. It gives reactive power compensation and harmonic elimination; it is fed into the single phase and given to the single phase VSI, which converts the DC into AC.
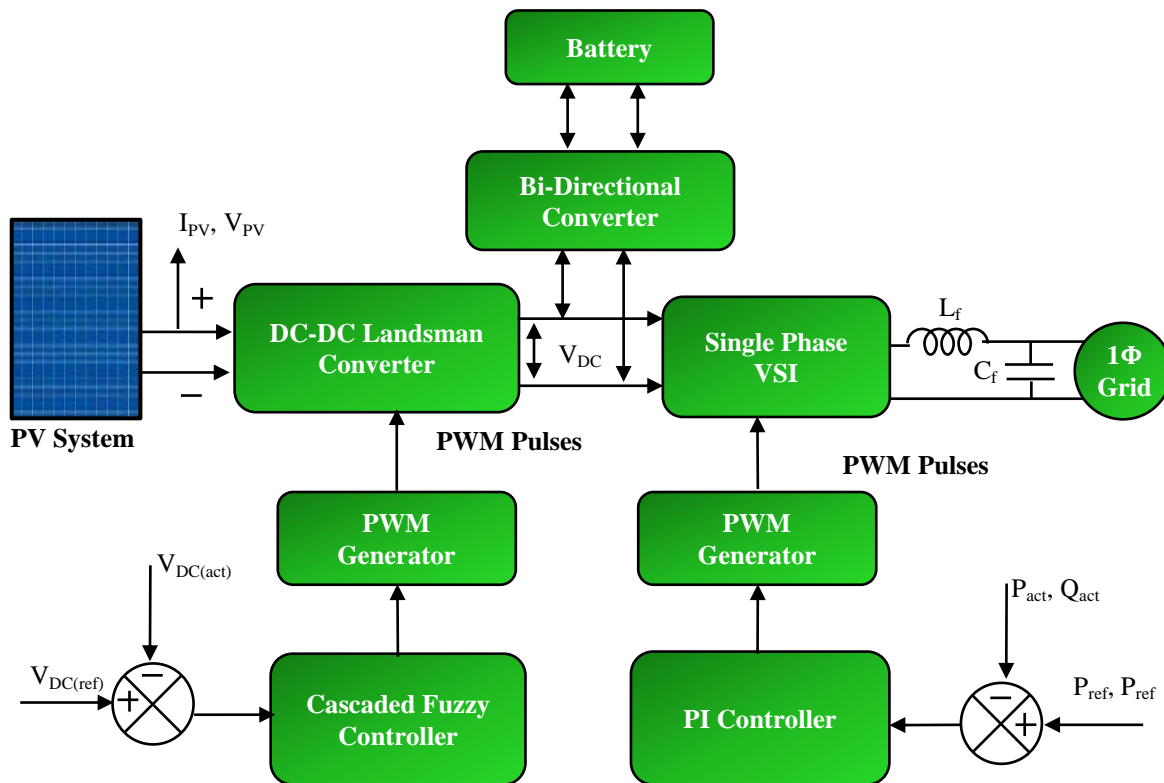

Fig. 1 Block diagram for the proposed work

The LC filter removes the harmonic distortion obtained in the VSI and maintains the sinusoidal output injected into the grid. The proposed work is depicted in Figure 1 as a block diagram.

2.1. Modelling of PV System
The fundamental part of a PV array is the solar cell. A small semiconductor layer is used to construct the p-n junction seen in solar cells, similar to p-n diodes. The solar cell can convert the photons from the sun into electrical energy.

$$I = Is\left(e^{(vd/nVt))} - 1\right) \quad (1)$$

$$I = I_l - I_d \quad (2)$$

Where n specifies the number of elements, Is denotes the saturation current, and Vt indicates the threshold voltage.

In Figure 2, the analogous circuit of the photovoltaic is displayed. The circuit comprises a diode, a parallel resistance, a photocurrent representing the leakage current, and a Series Resistance (R_S) that signifies the internal resistance of the PV cell. The voltage-current typical equation for a PV cell is given below.

A current source connected in parallel to a diode is used to simulate an ideal PV cell. Shunt and series resistances are included in the model, as indicated in the PV cell diagram because no solar cell is ideal. The inherent R_S has a meagre value. The analogous shunt resistance, or R_P, is exceptionally high.
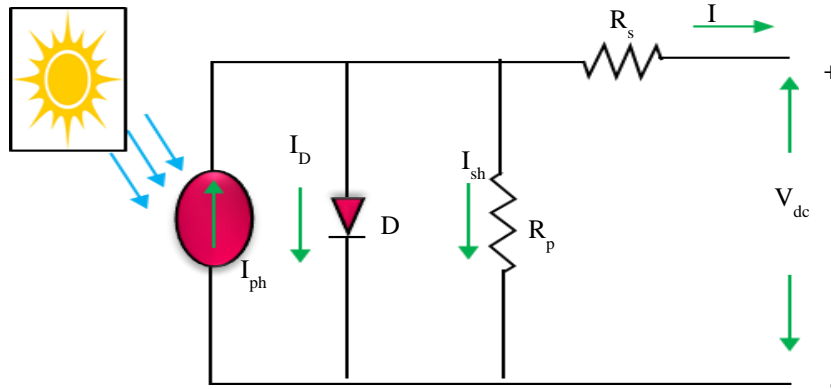

Fig. 2 Diagram of photovoltaic cell

Applying Kirchhoff's law to the node,

$$I_{ph} = I_d + I_{RP} + I \quad (3)$$

$$I = I_{ph} - I_d - I_{RP} \quad (4)$$

$$I = I_{ph} - I_o(e^{(v+IR\frac{s}{V_T}}\left(V + \frac{IR_s}{R_p}\right) \quad (5)$$

Where I indicates the cell current, V specifies the cell voltage, R_p represents the parallel resistance, I_{ph} denotes the photocurrent, I_0 shows the reverse saturation current, R_s indicates series resistance, T specifies temperature in kelvin.

The characteristics of P-V are expressed below,

$$I = I_{ph} - I_{os}\left[exp\left(\frac{V+RseL}{Vta}\right) - 1\right] - \frac{V+RseL}{Rpa} \quad (6)$$

The I_{ph} is produced directly by the incident of sunlight on a PV cell. The current fluctuates based on temperature, which is explained as,

$$I_{ph} = \left(I_{ph,n} + K_i\Delta T\right) \quad (7)$$

Where, K_i represents the coefficients of current temperature, ΔT denotes the variation between actual and nominal temperature.

2.2. Modelling of Landsman Converter
As shown in Figure 3, the Landsman converter is meant to operate in Continuous Conduction Mode (CCM) to minimize the current and voltage stresses on the power semiconductors device. The way it functions is examined by examining two modes and generating waveforms consistent with each mode.
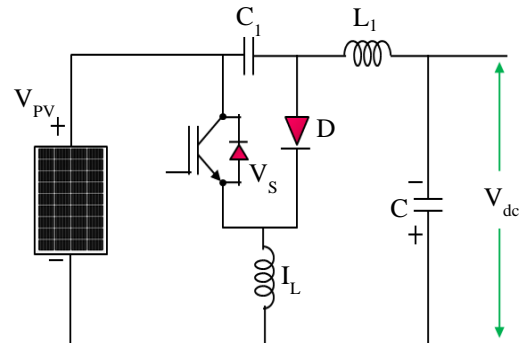

Fig. 3 Circuit diagram for the proposed landsman converter

2.2.1. Mode 1: Switch in ON Condition

The inductor current I_L Flow through the closed switch when the switch is in ON state and as V_{C1} is greater than the output voltage of V_{dc}, a reverse bias is generated in the diode. Through the switch, C_1 discharges, which send energy to the output and the inductor L. Thus, as shown in Figure 4 (a), V_{C1} falls and I_L rises as a result, energy is provided through the input to the input inductor L_1.

2.2.2. Mode 2: Switch in OFF Condition

A forward-biased diode conducts in the off state, subsequent in the circuit diagram illustrated in Figure 4 (b). Bypassing the inductor current I_L over the diode, energy stored in Mode I is converted into output power. Additionally, C_1 is charged by the energy received from both input and L_1. As a consequence, V_{C1} increases and I_L decreases, as illustrated in Figure mode 2.
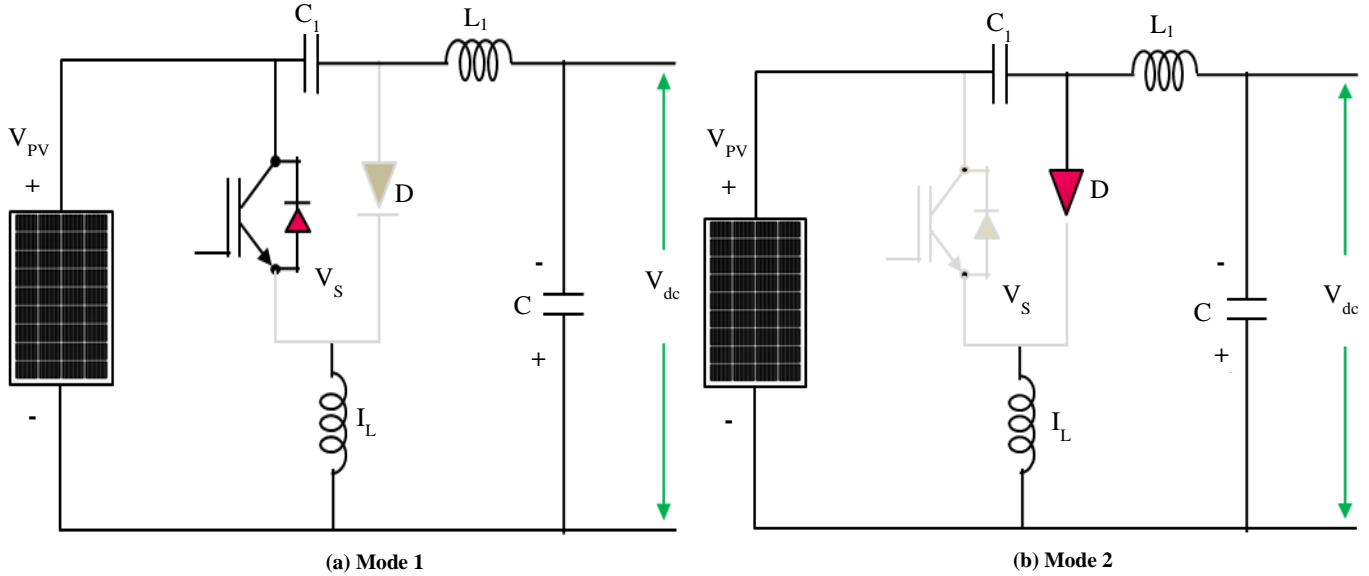

(a) Mode 1

(b) Mode 2

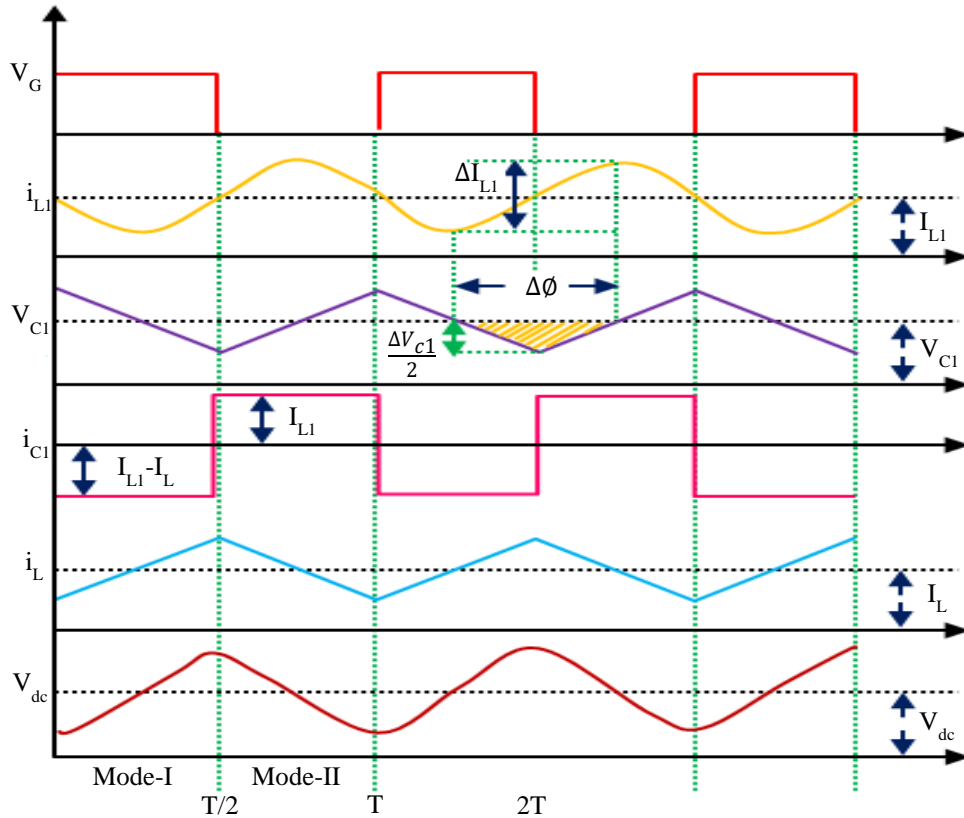**Fig. 4 Modes of operation (a) Mode 1, and (b) Mode 2.**

Fig. 5 Waveform for the landsman converter

As a result, the peak-to-peak current ripple flowing over L_1 is stated as follows:

$$\Delta I_{L_1} = \frac{\Delta \emptyset}{L_1} = \frac{1}{L_1}\frac{1}{2}\frac{\Delta V_{C1}}{2}\frac{T}{2} \qquad (8)$$

The current C_1 in mode 2 is expressed as,

$$I_{C_1} = I_{L_1} = C1\frac{\Delta V_{C_1}}{(1-D)T} \qquad (9)$$

Here, T specifies the switching time period, D indicates the duty cycle ratio. From eqn (2), the voltage ripple content in V_{C1} is calculated as follows,

$$\Delta V_{C_1} = \frac{1}{8L_1 C_1}\frac{I_{C_1}(1-D)}{f_{sw}^2} \qquad (10)$$

The aforementioned is normalized as follows:

$$\frac{\Delta I_{L_1}}{I_{L_1}} = \frac{1}{8L_1 C_1}\frac{(1-D)}{f_{sw}^2} \qquad (11)$$

Here, the switching frequency is specified as $f_{sw} = 1/T$

$$I_{L_1} = \frac{D}{1-D}I_{dc} \qquad (12)$$

Sub I_{L_1} in eq (9)

$$L_1 = \frac{DI_{dc}}{8f_{sw}^2 C_1 \Delta I_{L_1}} \qquad (13)$$

2.3. Cascaded Fuzzy Controller

The Landsman converter performs dynamically better using an appropriate controller, such as CFLC, which allows error correction. Cascaded control enables speedy responses to interruptions and ensures whole system control. In the current work, fuzzy cascade control structures are designed as well as used because fuzzy sets are very effective at addressing the issue of uncertainty as well as non-linearity in a system. The suggested cascaded control approach consists of two FLCs coupled in series, as depicted in Figure 6.

The second FLC is driven by the reference control signal from the first FLC to produce the required duty cycle ΔD command for controlling the converter's switching pulses. The second FLC is utilized to reduce distortions because it harms the Landsman converter's output.
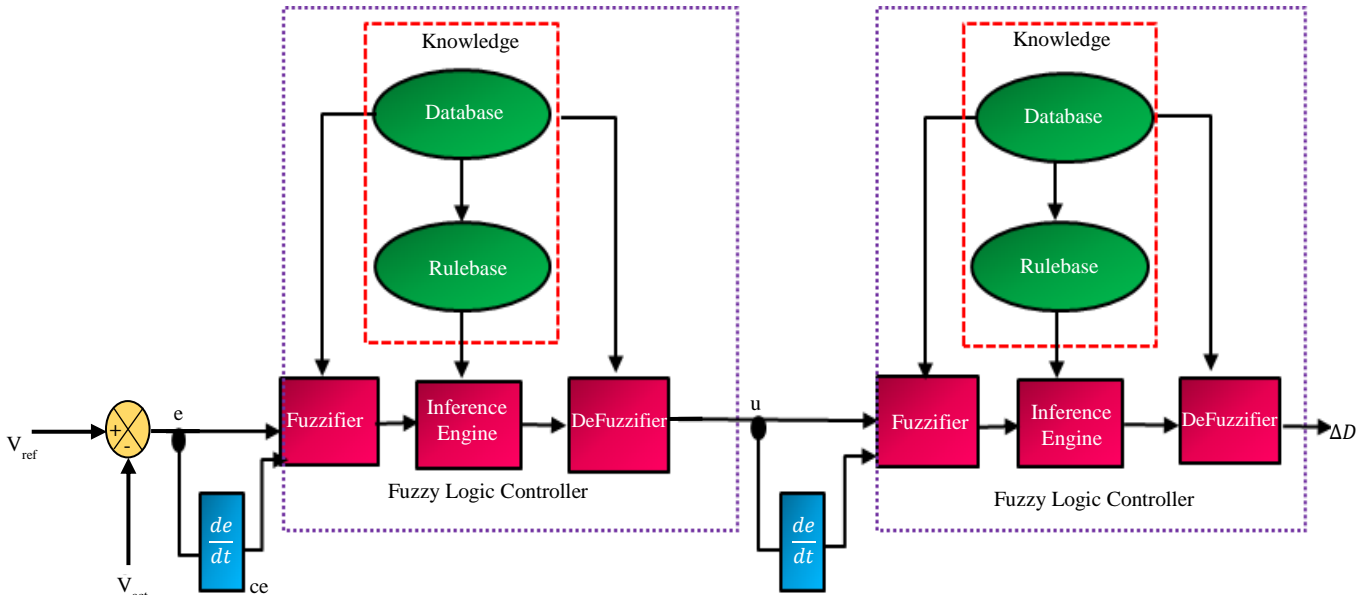

Fig. 6 Architecture of CFLC

An error E is calculated by comparing the converter's voltage output. V_{act}, to the reference voltage V_{dc}. The CFLC receives input from error E and the change in error ΔE.

The PWM is then provided with the CFLC-optimized output to deliver the necessary pulses for effectively increasing converter output. The CFLC approach employed in this study is a closed-loop control technique, which

is utilized to keep the Photovoltaic system's output voltage constant.

The CFLC rule base is illustrated in Figure 7 and Table 1, along with the triangle membership functions of the inputs E and ΔE. Fuzzy linguistic variables typically represent the rule basis. The k-th linguistic control rule for the intended 7×7 rule base is provided as,
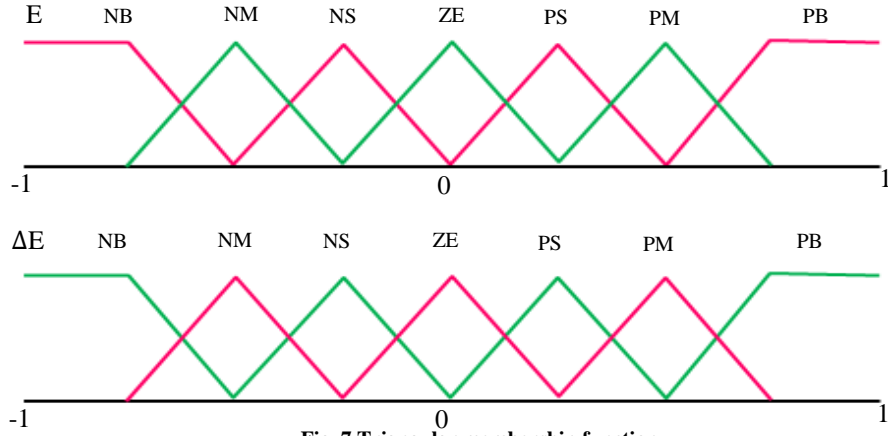
Fig. 7 Triangular membership function

Table 1. CFLC rule base

E / Δ E	NB	NM	NS	ZO	PS
NB	PB	PB	PB	PB	PM
NM	PB	PB	PB	PM	PS
NS	PB	PB	PM	PS	Z
ZO	PB	PM	PS	Z	NS
PS	PM	PS	Z	NS	NM
PM	PS	Z	NS	NM	NB
NM	Z	NS	NM	NB	NB

Where the change in error is indicated as ΔE_k, the k-th rule is denoted as R^k, the error represents the E_k. B_k And A_k is specified as the change in error and the linguistic value of error correspondingly.

2.4. Single Phase VSI

A single-phase inverter circuit is used to analyze the work characteristics to facilitate analysis. According to KCL and KVL law, the inverter's output current is given below,

$$i_L = i_c + i_o \tag{14}$$

$$U_i = U_L + R_{iL} + U_O = j\omega L + R_{iL} + U_O \tag{15}$$

The inverter output voltage is given as,

$$U_O = R_{cic} + \frac{1}{j\omega C} i_c \tag{16}$$

The inverter output transfer function is given as,

$$P(s) = \frac{U_o(s)}{U_i(s)} = \frac{\left(\frac{1}{sC} + R_c\right)//R_o}{(sL+R) + \left(\frac{1}{sC+R_c}\right)//R_o} \tag{17}$$
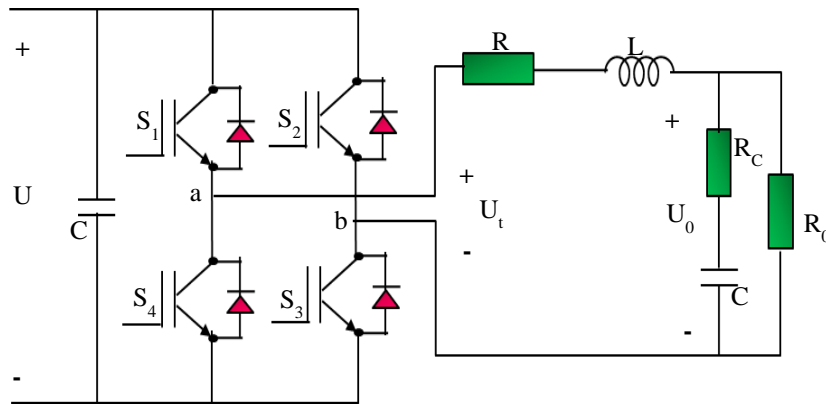

Fig. 8 Structure of single-phase VSI

Figure 8 demonstrates that the inverter is a nonlinear circuit with an increased output impedance; the presence of a nonlinear circuit with an output impedance cause the system to be distorted, resulting in a sequence of spikes in the output current.

2.5. Modeling of Bidirectional Converter for Battery

The non-isolated bidirectional DC-DC converters are specified in Figure 9. The converter operates in two modes. Here, controlled switches are used instead of diodes to enable bidirectional operation.

2.5.1. Buck Mode

The output voltage is less than the input voltage in Buck mode. Switch S1 has to be activated, and S2 has to be maintained OFF to charge the battery from the DC grid. The input current rises and passes over switch S1 and L when switch S1 is ON. The inductor current decreases till the next cycle when S1 is OFF. The battery is charged using the energy stored in inductor L.

2.5.2. Boost Mode

In Boost mode, the output voltage has a higher value than the input voltage. Power from the battery is discharged to the load when switch S2 is activated, and S1 is off.

When switch S2 is turned ON, inductor L and switch S2 undergo an increase in input current. The inductor current decreases till the next cycle when S2 is OFF. Energy from inductor L flows through the load.
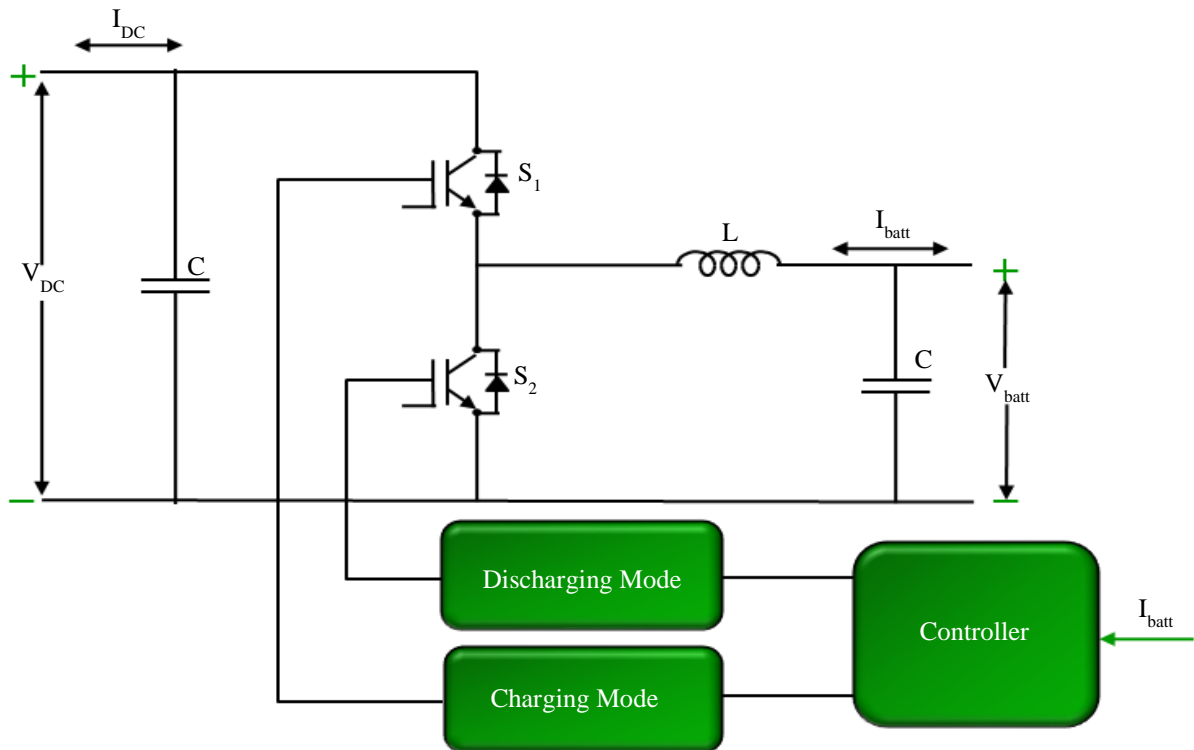

Fig. 9 Bidirectional converter for battery

3. Results and Discussion

This study proposes the optimal designs for Photovoltaic (PV) systems BEES. The MATLAB software simulates the output of the proposed technique. As a result, the suggested approach attains a Low THD value by using the Landsman converter compared to the other conventional converters. The proposed method's simulation and comparison graphs are discussed below, and the parameter specification is represented in Table 2.

PV panel voltage waveform is represented in Figure 10 (a), which is observed that initially, the voltage is maintained constant at 45.6V. After 0.1s, the voltage is suddenly raised and maintained constant voltage at 47.8V. Figure 10 (b) represents the converter input current waveform; from figure, it is analyzed that initially, the current fluctuated with minor distortion. After 0.3s, the current is constantly maintained at 240A.

The converter output voltage waveform is represented in Figure 11 (a), which is observed that initially, the voltage varies with minor distortion; after 0.3s, the voltage is constantly maintained at 610V. Figure 11 (b) illustrates the converter output current waveform. From the Figure 11(b), It is noted that the current fluctuated initially; after 0.3s, the current is maintained constant at 15A.

Table 2. Parameters specifications

Parameters	Description
Solar PV System	
Open Circuit Voltage	12V
Peak Power	10KW, 10 Panels
Short Circuit Current	8.3A
Series Connected Solar Panel	36
Landsman Converter	
L_1, L_2	1µH
C_1, C_2	4.7µF,22µF
Switching Frequency	10KHz
R_o	50Ω

(a)   (b)
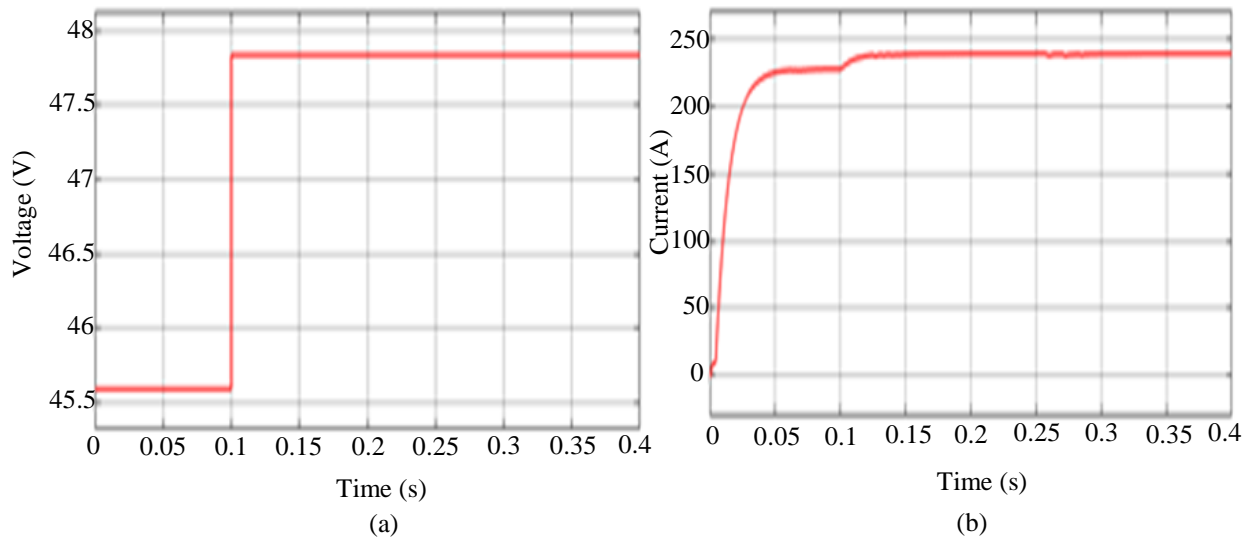
Fig. 10 PV panel input (a) Voltage, and (b) Current waveform.

(a)   (b)
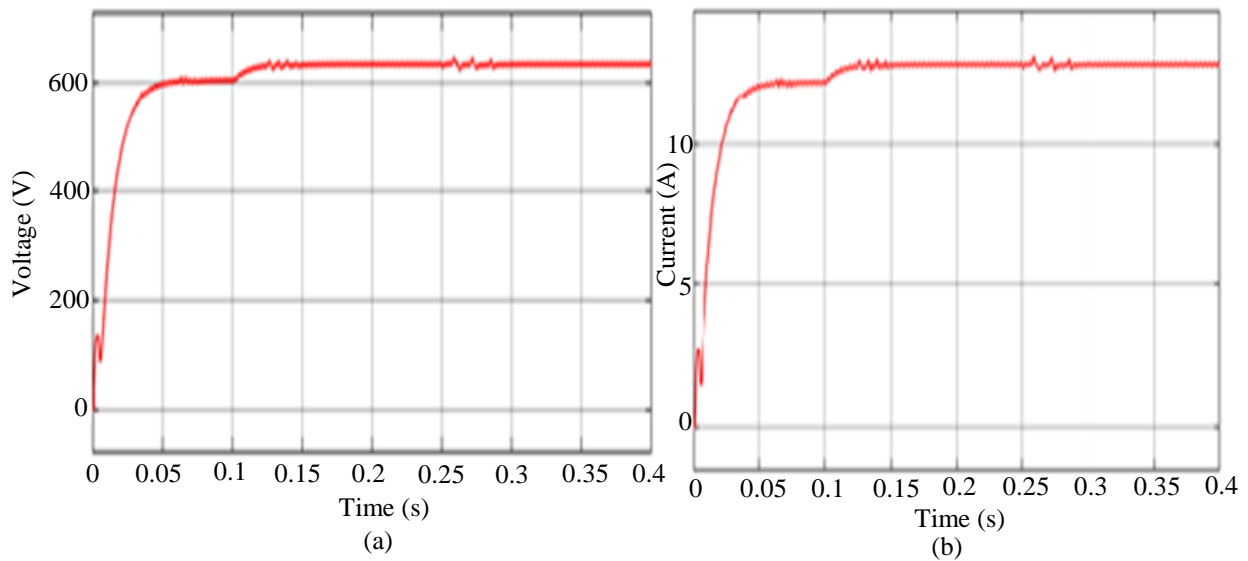
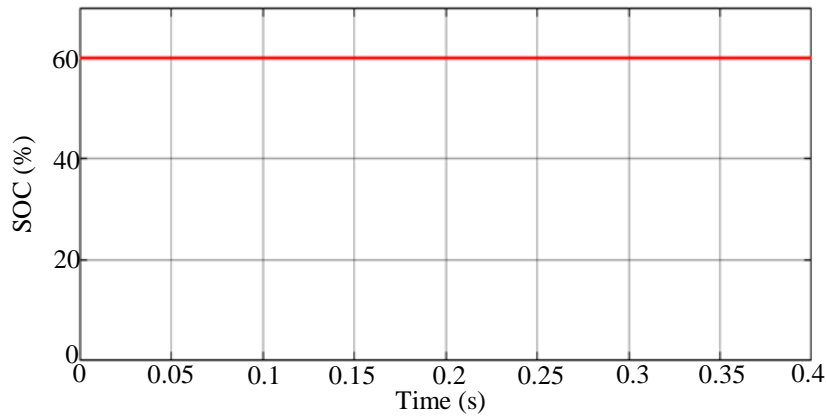**Fig. 11 Converter output (a) Voltage, and (b) Current waveform.**

Fig. 12 Battery SOC waveform

Battery SOC waveform is illustrated in Figure 12, which is analyzed that the SOC is constantly maintained at 60%.

Figure 13 (a) represents the battery voltage waveform, which is observed that the voltage is constantly maintained at 12.5, as specified in the below figure. Battery current waveform is specified in Figure 13 (b), from figure it is analyzed that initially current varies; after 0.25s, the voltage is maintained constant at 1.5A. Figure 14 (a) specifies the grid voltage waveform, which is noted that the voltage is constantly maintained at 370V to -370V. The grid current waveform is represented in Figure 14 (b); from Figure, it is analyzed that the current is constantly maintained at 11A to -11A. Figure 15 (a) illustrates the accurate power waveform, which is observed that the power initially fluctuated with minor distortion; after 0.1s, the power is constantly maintained at 5750W. The reactive power waveform is specified in Figure 15 (b), which initially varies with high distortion; after 0.3s, the power is constantly maintained at -70 to -150VAR.
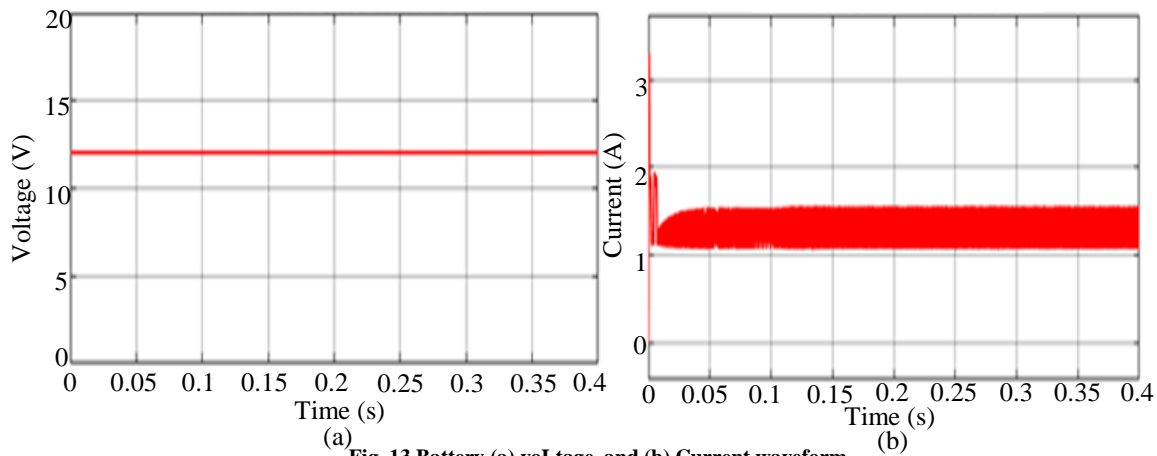

(a)

(b)

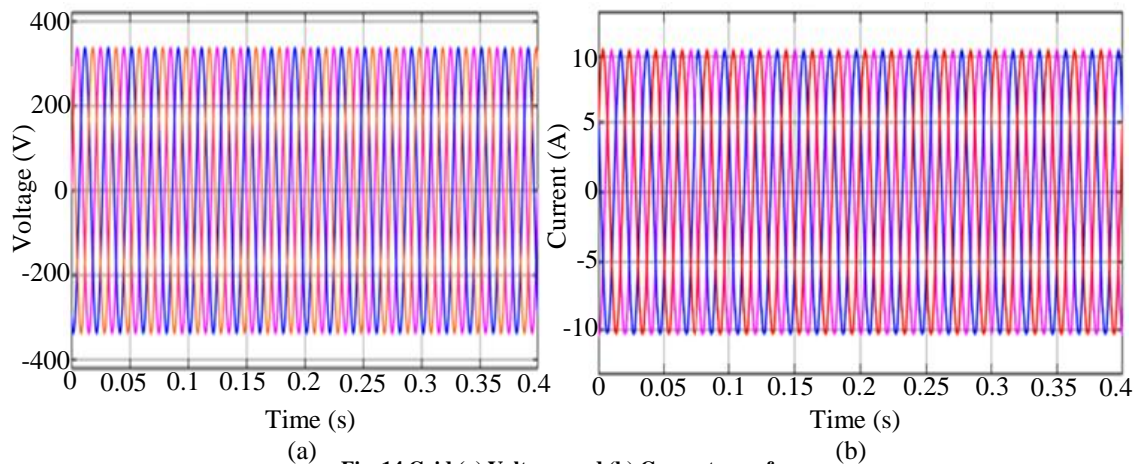**Fig. 13 Battery (a) voLtage, and (b) Current waveform.**

(a)

(b)

Fig. 14 Grid (a) Voltage, and (b) Current waveform.

Fig. 15 (a) Real, and (b) reactive power waveform.

Fig. 16 Power factor waveform
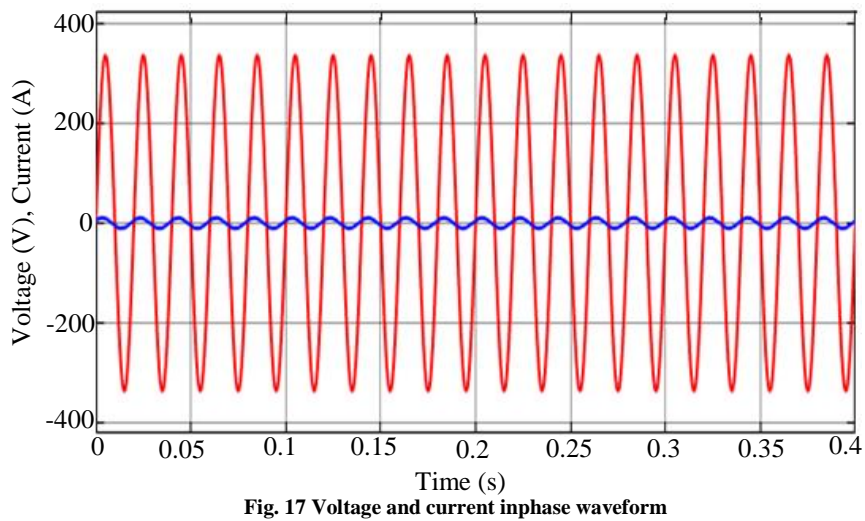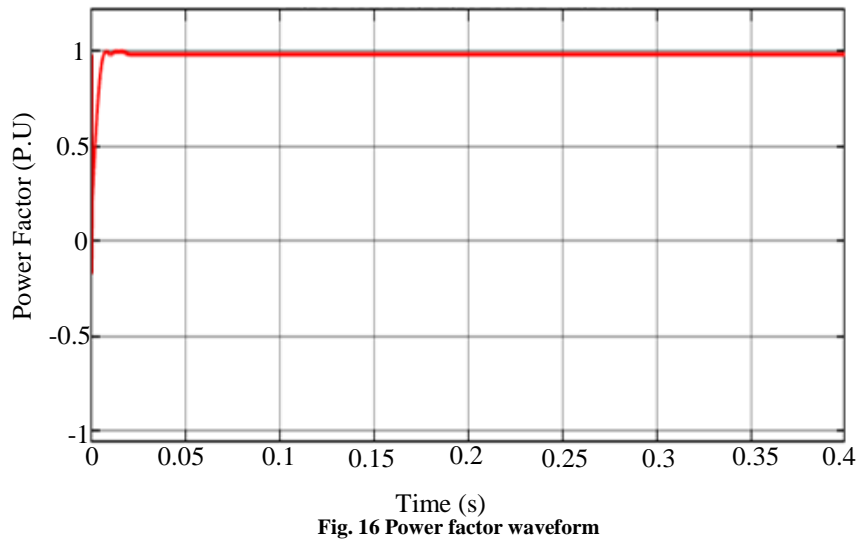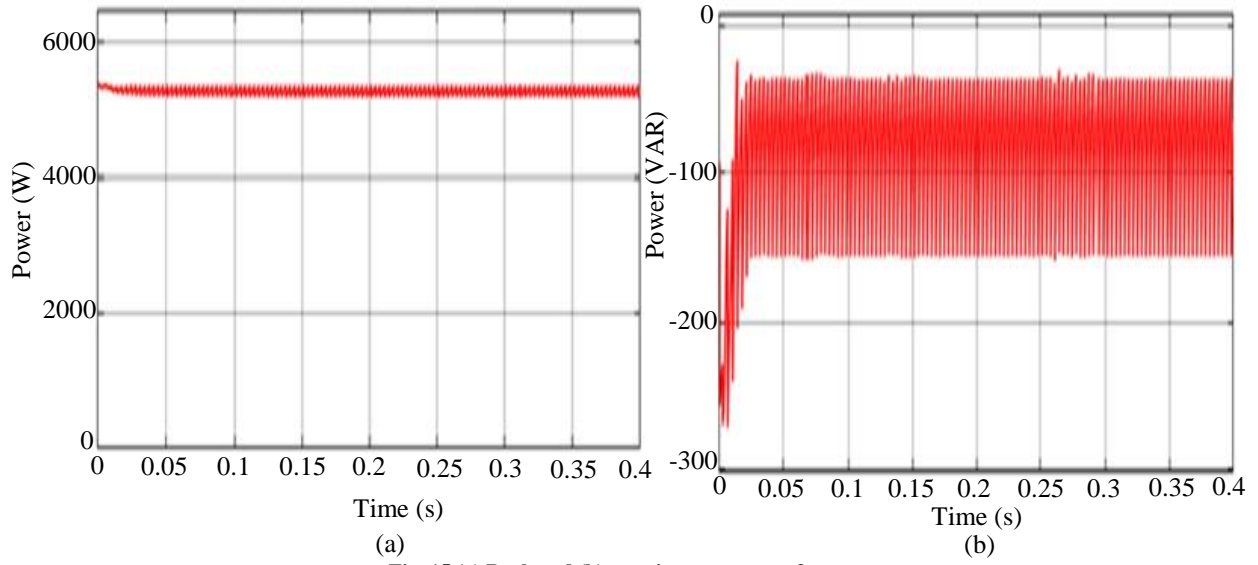

Fig. 17 Voltage and current inphase waveform

Figure 16 specifies the power factor waveform; from figure, it is noted that the power factor initially fluctuated and suddenly raised at 1P.U after 0.05s.

Voltage and current in phase waveform are represented in Figure 17, which is observed that the voltage and current are constantly maintained at 370A to -370A and 0A as specified above in Figure.

The THD value for the suggested method is illustrated in Figure 18, from figure it is noted that the THD value is obtained at 1.24%, which is lower than the conventional techniques.

Figure 19 represents the comparison of THD value, which is analyzed how the proposed technique is compared to the conventional approaches.

The suggested technique of the landsman converter achieves 1.24%, which is a low THD value than the existing converters like Buck-boost, Cuk, SEPIC, and Luo by the efficiency of 3.24%, 3.12%, 2.19% and 2.03%.
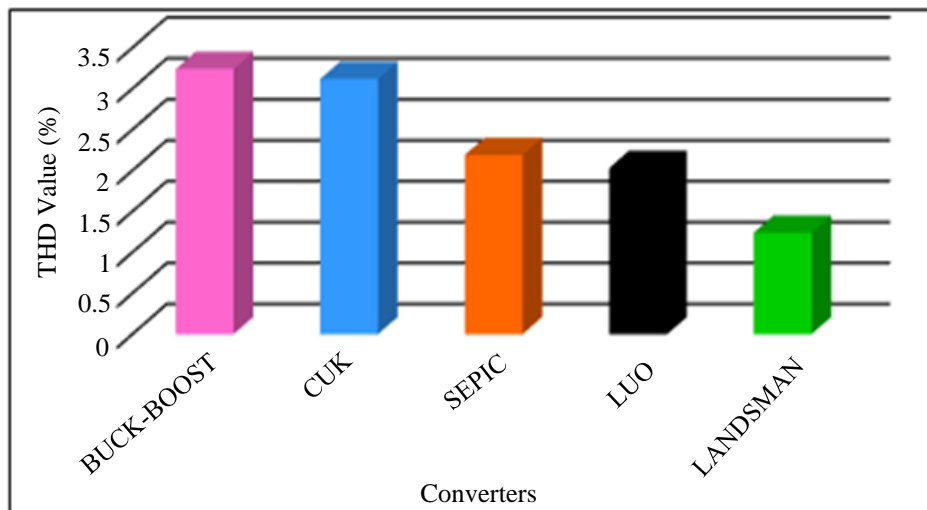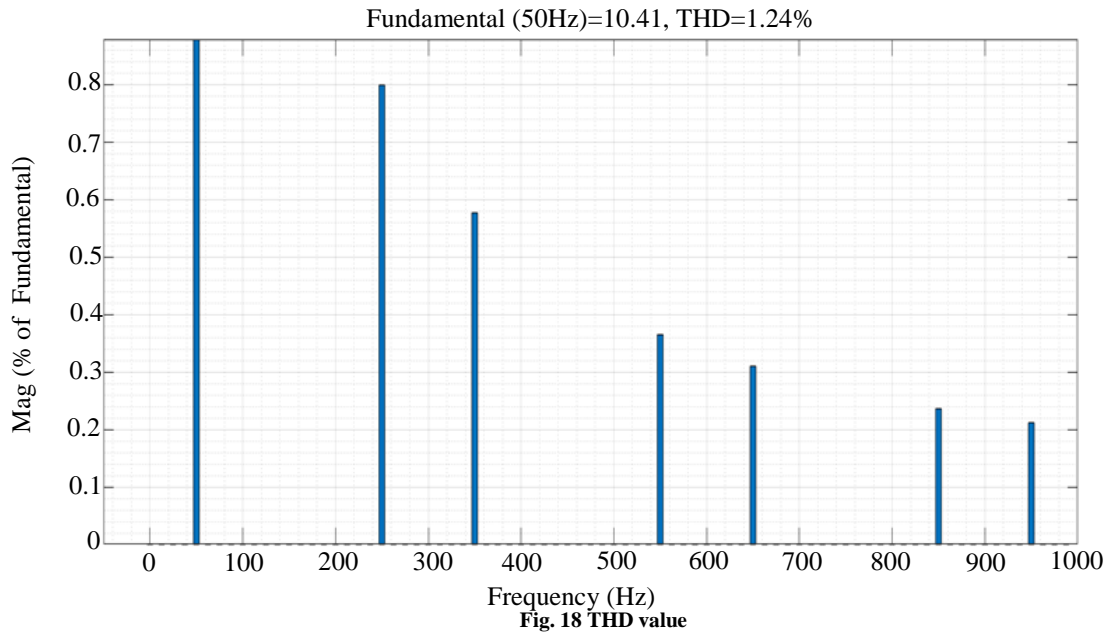
Fundamental (50Hz)=10.41, THD=1.24%

Fig. 18 THD value

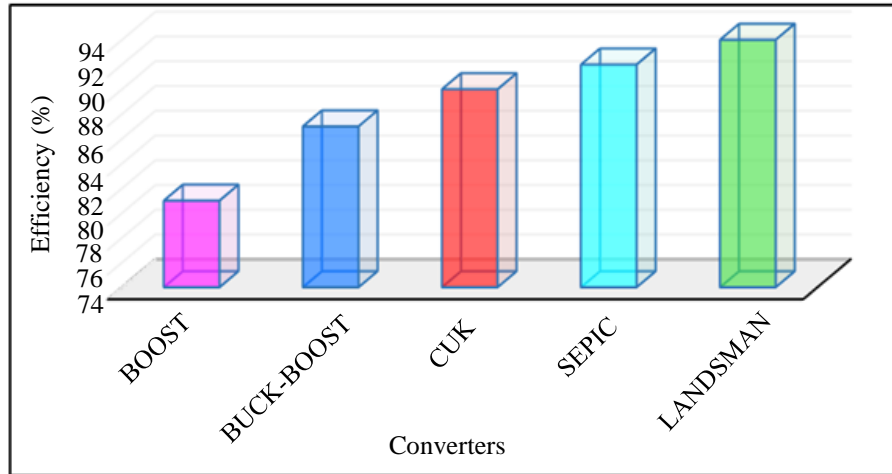**Fig. 19 Comparison of THD value (%)**

Fig. 20 Comparison of efficiency

The efficiency comparison is represented in Figure 20, which shows that the proposed Landsman converter achieves a high efficiency of 94% compared to conventional converters like Boost, Cuk, Buck-Boost, and SEPIC.

Figure 21 specifies the comparison of voltage gain; from the graph, it is analyzed that the voltage gain for the proposed Landsman converter attains high by the ratio of 1:12 compared to the existing converters.
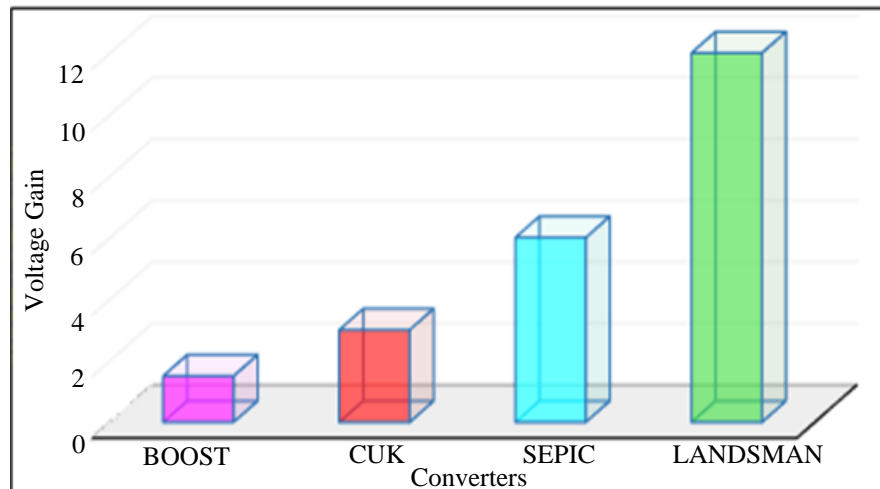

Fig. 21 Comparison of voltage gain

4. Conclusion

This paper proposes a grid-connected PV system with BEES to provide uninterrupted supply to the grid. The landsman converter is utilized in this work to increase the DC voltage from the PV system. A Cascaded Fuzzy controller regulates the converter's switching operation, stabilizing the voltage and improving the dynamic performance by compensating for errors. Furthermore, a PI controller is implemented on the grid side to reduce the system stability's steady-state error and enhance the grid performance. The MATLAB software simulates the overall framework, and the corresponding results are contrasted with other state-of-the-art approaches. The suggested landsman converter achieves a 1.24% THD value, which is lower than the existing converters. The proposed Landsman converter achieves a high efficiency of 94% and voltage gain by the ratio of 1:12, which is high compared to the other conventional converters.

References

[1] Vishnu Mahadeva Iyer et al., "An Approach Towards Extreme Fast Charging Station Power Delivery for Electric Vehicles with Partial Power Processing," *IEEE Transactions on Industrial Electronics*, vol. 67, no. 10, pp. 8076-8087, 2020. [CrossRef] [Google Scholar] [Publisher Link]

[2] P. Prem et al., "Fast Charging Converter and Control Algorithm for Solar PV Battery and Electrical Grid Integrated Electric Vehicle Charging Station," *Automation Journal for Control, Measurement, Electronics, Computing and Communications*, vol. 61, no. 4, pp. 614-625, 2020. [CrossRef] [Google Scholar] [Publisher Link]

[3] Heena Parveen, and A. Raghu Ram, "A PSO-ANFIS MPPT-Based 3-Phase Series Resonant Converter with DLLC Tanks for Hybrid Solar Wind Battery System with DC-Load," *SSRG International Journal of Electrical and Electronics Engineering*, vol. 10, no. 7, pp. 199-210, 2023. [CrossRef] [Publisher Link]

[4] Sabrina Yeasmin, Tushar Kanti Roy, and Subarto Kumar Ghosh, "Design of Robust Integral Terminal Sliding Mode Controllers with Exponential Reaching Laws for Solar PV and BESS-Based DC Microgrids with Uncertainties," *Sustainability*, vol. 14, no. 13, pp. 1-17, 2022. [CrossRef] [Google Scholar] [Publisher Link]

[5] Pasquale Franzese et al., "Optimized Control Strategy for Single-Phase Multilevel Cascaded Converter in a Distributed PV-BESS System," *Electric Power Systems Research*, vol. 214, p. 108818, 2023. [CrossRef] [Google Scholar] [Publisher Link]

[6] Yong-Rae Lee, Hyun-Joon Kang, and Mun-Kyeom Kim, "Optimal Operation Approach with Combined BESS Sizing and PV Generation in Microgrid," *IEEE Access*, vol. 10, pp. 27453-27466, 2022. [CrossRef] [Google Scholar] [Publisher Link]

[7] Saman Korjani et al., "An Online Energy Management Tool for Sizing Integrated PV-BESS Systems for Residential Prosumers," *Applied Energy*, vol. 313, p. 118765, 2022. [CrossRef] [Google Scholar] [Publisher Link]

[8] Adedayo Owosuhi, Yskandar Hamam, and Josiah Munda, "Maximizing the Integration of a Battery Energy Storage System–Photovoltaic Distributed Generation for Power System Harmonic Reduction: An Overview," *Energies*, vol. 16, no. 6, pp. 1-22, 2023. [CrossRef] [Google Scholar] [Publisher Link]

[9] A. Dominic Savio, and Vimala Juliet A, "Development of Multiple Plug-in Electric Vehicle Mobile Charging Station using Bidirectional Converter," *International Journal of Power Electronics and Drive Systems*, vol. 11, no. 2, pp. 785-791, 2020. [CrossRef] [Google Scholar] [Publisher Link]

[10] Ziyi Zhao, "Operation Simulation and Economic Analysis of Household Hybrid PV and BESS Systems in the Improved TOU Mode," *Sustainability*, vol. 15, no. 11, pp. 1-23, 2023. [CrossRef] [Google Scholar] [Publisher Link]

[11] Sajib Chakraborty et al., "DC-DC Converter Topologies for Electric Vehicles, Plug-in Hybrid Electric Vehicles and Fast Charging Stations: State of the Art and Future Trends," *Energies*, vol. 12, no. 8, pp. 1-43, 2019. [CrossRef] [Google Scholar] [Publisher Link]

[12] Emad Awada, Eyad Radwan, and Mutasim Nour, "Robust Sliding Mode Controller for Buck DC Converter in Off-Grid Applications," *Bulletin of Electrical Engineering and Informatics*, vol. 11, no. 5, pp. 2425-2433, 2022. [CrossRef] [Google Scholar] [Publisher Link]

[13] R. Palanisamy et al., "Simulation of Various DC-DC Converters for Photovoltaic System," *International Journal of Electrical and Computer Engineering*, vol. 9, no. 2, pp. 917-925, 2019. [CrossRef] [Google Scholar] [Publisher Link]

[14] Carlos Andres Ramos-Paja, Juan David Bastidas-Rodriguez, and Andres Julian Saavedra-Montes, "Low-Voltage Photovoltaic System Based on a Continuous Input/Output Current Converter," *Computation*, vol. 11, no. 2, pp. 1-30, 2023. [CrossRef] [Google Scholar] [Publisher Link]

[15] Julio López Seguel, Seleme I. Seleme, and Lenin M. F. Morais, "Comparative Study of Buck-Boost, SEPIC, Cuk and Zeta DC-DC Converters using Different MPPT Methods for Photovoltaic Applications," *Energies*, vol. 15, no. 21, pp. 1-26, 2022. [CrossRef] [Google Scholar] [Publisher Link]

[16] Abhilash Narasimhan, "Cuk-Based Single-Phase Inverter Design for PV Array Systems," *Renewable Energy Optimization, Planning and Control*, Singapore, pp. 139-148, 2022. [CrossRef] [Google Scholar] [Publisher Link]

[17] Ratna Ika Putri, Surya Nata, and Bambang Priyadi, "Battery Charging Control using Photovoltaic with Sepic Converter," *International Journal of Frontier Technology and Engineering*, vol. 1, no. 1, pp. 33-41, 2022. [CrossRef] [Google Scholar] [Publisher Link]

[18] Rini Nur Hasanah et al., "Design of PI Sliding Mode Control for Zeta DC-DC Converter in PV System," *Bulletin of the Polish Academy of Sciences Technical Sciences*, vol. 70, no. 3, pp. 1-8, 2022. [CrossRef] [Google Scholar] [Publisher Link]

[19] Ahmed Darwish, "A Bidirectional Modular Cuk-Based Power Converter for Shore Power Renewable Energy Systems," *Energies*, vol. 16, no. 1, pp. 1-28, 2023. [CrossRef] [Google Scholar] [Publisher Link]

[20] Waleed Khaled Abdulrazaq Abdulrazaq, and Ahmet Mete Vural, "Fuzzy Fractional-Order PID Control for PMSG Based Wind Energy Conversion System with Sparse Matrix Converter Topology," *International Transactions on Electrical Energy Systems*, vol. 2022, pp. 1-18, 2022. [CrossRef] [Google Scholar] [Publisher Link]

[21] Sarfaraz Nawaz Syeda, and S. Tara Kalyani, "Performance Analysis of DFIG with PI, PID and FOPID Control Schemes in Micro Grid," *Turkish Journal of Computer and Mathematics Education*, vol. 13, no. 2, pp. 184-194, 2022. [Google Scholar] [Publisher Link]

[22] E. Parimalasundar et al., "Performance Analysis of a Seven-Level Multilevel Inverter in Grid-Connected Systems," *SSRG International Journal of Electrical and Electronics Engineering*, vol. 10, no. 6, pp. 9-22, 2023. [CrossRef] [Publisher Link]

[23] Sameh Mahjoub et al., "Design and Implementation of a Fuzzy Logic Supervisory Based on SMC Controller for a Dual Input-Single Output Converter," *International Journal of Electrical Power & Energy Systems*, vol. 150, p. 109053, 2023. [CrossRef] [Google Scholar] [Publisher Link]